A highly-sensitive automatic transient laser-induced breakdown spectroscopy system with high temporal and spatial resolution*

Liu Qiao-Jun(刘巧君)[a)b)], S. K. Fong(冯瑞权)[c)], Andrew Y. S. Cheng(郑玉臣)[a)b)†], Luo Shi-Rong(罗时荣)[a)], K. S. Tam(谭建成)[c)], Zhu Jian-Hua(朱建华)[a)], and A. Viseu(冼保生)[c)]

[a)] *Department of Physics, Sichuan University, Chengdu* 610064, *China*

[b)] *Faculty of Information Technology, Macau University of Science and Technology, Macao Special Administrative Region (SAR), China*

[c)] *Meteorological and Geophysical Bureau, Macao Special Administrative Region (SAR), China*

(Received 5 September 2011; revised manuscript received 14 October 2011)

A highly-sensitive automatic transient laser-induced breakdown spectroscopy (LIBS) system is designed and integrated. It successfully avoids the delay time selecting problem in the conventional LIBS system, and realizes the LIBS data acquisition with high spatiotemporal resolution automatically. Multiple transient spectra can be obtained in each measurement, which will provide more information for spectral research. The water–vapour and liquid–water Raman scattering spectra are captured by this system, and the comparison of experimental water–vapour Raman scattering spectrum with theoretical data verifies the reliability of the LIBS system. Based on this system, the air laser induced air breakdown spectra are captured and analysed. The system is also useful for the research on water–vapour Raman Lidar remote sensing.

Keywords: laser-induced breakdown spectroscopy, water Raman spectrum, water–vapour Raman Lidar

PACS: 74.25.nd, 42.60.–v, 42.62.–b **DOI:** 10.1088/1674-1056/21/8/087402

1. Introduction

Laser induced breakdown spectroscopy (LIBS) is an excellent laser-based atomic emission spectroscopy employing an energetic laser pulse as the excitation and ionization source. LIBS has advantages over other analysis methods, since it provides real-time quasi non-intrusive determination of the elemental compositions and quantities of the substance in a quick and user-friendly way.

The laser induced breakdown spectrum can be observed in gaseous, liquid, and solid samples,[1] which permits the real time multi-element analysis. The application of LIBS has progressed tremendously in the last decade. It could be employed in a rarefied atmosphere for analysing elements on silicate minerals.[2] With minimal sample preparation,[3] a rapid analytical response to the concentration of metal pollutants in soils was provided. The non-contact property extends the application of LIBS to atmospheric exploration such as the monitoring of aerosols in ambient air.[4] This makes LIBS easily connected with Raman scattering for atmospheric condition analysis.[5,6] The excitation of Raman scattering requires high energy, and so does the LIBS system. For the high laser emitted energy in a LIBS system, researchers used it to record Raman scattering spectrum. Sharma *et al.*[7] performed mineral analysis through Raman scattering and LIBS, and they adjusted the laser power electronically and changed photon flux density at the sample by varying the spot diameter for Raman measurement and combined LIBS and Raman measurements.

The LIBS technique can also be used to research the phase shift of the interference fringes produced in water,[8] perform the tap water analysis of elements' dissolved cations,[9] investigate plasma recombination emissions and spectral blueshift,[10] execute elemental analysis, and so on.[11–14] The dual beam arrangement has also been designed and employed.[15,16]

Although the LIBS technique has widespread applications in the elemental analysis, there is still an

*Project supported by the Macao Science and Technology Development Fund, Macao Special Administrative Region (SAR), China (Grant No. 021/2007/A2) and the National Natural Science Foundation of China (Grant No. 11176019).

†Corresponding author. E-mail: ayscheng@netvigator.com

© 2012 Chinese Physical Society and IOP Publishing Ltd

adjustment problem which needs to be taken into consideration. The LIBS emission is mainly composed of two parts.[17] One part is highly inhomogeneous and specific line distribution at a certain wavelength which gives the interested information. The other is the continuum emission for all the spectral domains which rapidly decays in typical LIBS plasmas to become negligible after a few hundreds of nanoseconds. LIBS systems are used to detect trace elements in a mixture, which always has a weaker signal. In a traditional LIBS system ICCD is used as a spectral collecting component because it is more sensitive to capturing weak lines. However, the drawback of ICCD is lacking in spatiotemporal resolution. One can only collect a single transient spectrum in each measurement. In order to avoid the specific lines of trace elements, submerged by continuum emission, and obtain a higher signal-to-noise ratio, a delay time after the laser firing is needed for the ICCD acquisition system. The appropriate delay time evaluated between the emission of continuum radiation and characteristic radiation is important. The ICCD acquisition will be executed after the selected delay time to avoid the influence of continuum emission. In our new highly-sensitive automatic transient LIBS system, we properly solve the delay-time selecting problem by using a photomultiplier tube (PMT) and transient recorder to replace ICCD. The PMT, with a high sensitivity, could amplify the weak photons of the plasma spectral intensity. The transient recorder has an excellent spatiotemporal resolution, and it could obtain the spectral intensity changes with time and wavelength at the same time. This PMT and transient recorder acquisition system promises a more detailed and comprehensive understanding of spectrum and overcomes the delay-time selecting shortcoming in the traditional ICCD system. Multiple transient spectra can be collected in each measurement. Individual spectral line features can be easily distinguished from the continuous spectrum by choosing an appropriate higher signal-to-noise ratio (SNR) moment. In application, researchers can easily select the required spectrum at any time after the laser firing. The automatic design is convenient for researchers to capture and analyse the spectra. This is an important technological innovation in our system.

The rest of this paper is organized as follows. In Section 2, we describe this highly-sensitive automatic transient LIBS system. By comparing the experimental Raman spectrum of water vapor with that obtained from theoretical calculation, the system was tested. Applying this new system, the laser induced air breakdown spectrum was captured and analyzed. The measurement cases and discussion are presented in Section 3, while Section 4 gives the conclusion.

2. LIBS system set-up

The schematic plot of the highly-sensitive automatic transient LIBS system set-up is shown in Fig. 1. A laser beam emitted by Nd:YAG laser source is focused by a quartz lens with a short focal length of 100 mm to generate the laser-induced breakdown emission spectrum at the focal spot.

An optical fiber, together with a collimating lens located near the focal spot in the direction perpendicular to the laser beam, is used to collect the plasma light. The light propagating through the fiber is then focused on the entrance slit of the monochromator via a relay lens. Traditionally, researchers also used a spectrograph as the spectrum capturing tool, which is insensitive to weak signals and lacking in spatiotemporal resolution, and it is necessary to gate the detector. In order to optimize the performance of the LIBS system, we use the combination of a monochromator, a PMT and a transient recorder to replace the traditional gated spectrograph. The monochromator has a wide spectral range with interchangeable grating, high throughput, low stray light, and changeable slit width which leads to a selectable spectral resolution. The PMT has high-sensitivity, which is located at the exit slit of the monochromator, amplifies the weak photons of the plasma spectral intensity and finally the output signal is captured using the transient recorder in tandem with a computer.

The central wavelength of the monochromator can be changed by the rotatable grating through the gear and computer controlled stepper motor. In this system, wavelength scanning can be automated using the control software; each step of the stepper motor changes the central wavelength by 0.0625 nm. The transient recording data acquisition system is optimized for fast repetitive photomultiplier signals in a voltage range of 0–500 mV. The signal is recorded simultaneously by a 12-bit, 40-MHz analog to digital converter and a selected threshold photon counting detection electronics. The combination of analog and photon counting detection can provide a very large dynamic range. Compared with a traditional spectrograph which can only give the intensity information

about the spectrum, the transient recorder has an excellent spatiotemporal resolution. So, users can also take LIBS measurements at a distance with appropriate front–end optical assembly. This feature has great advantage especially for a remote sensing measurement scenario. After each data averaging cycle of the transient recorder, the computer can change the central wavelength of the monochromator in the desired wavelength interval via the stepper motor controller, and then repeat the next data acquisition cycle. In this way, the spectral acquisition of the plasma emission can be repeated automatically for a designed spectral range with excellent accuracy.

This LIBS system is first tested by measuring the liquid–water and water–vapour Raman scattering signals. As is well known, water plays an important role in the hydrological and material cycles of the earth's atmosphere. By absorbing and emitting radiation in the infrared region, it participates in the radiation balance of the earth. As one of the most effective greenhouse gases, water vapour can form cloud particles through condensation on aerosols, and evaporate from them to moisten the air. The conversion and transport between liquid water and water vapour has also received much attention in the past decade. The detection of water–vapour and liquid–water signals in the atmosphere has become a subject of intense research and laser has become one of the leading technologies used in the atmospheric remote sensing.[18−23] The Raman spectra of liquid water and water vapour can be simulated by quantum theory.[24,25]

In the experiment, the centre of a tube of distilled water was located at the focal spot in Fig. 1. The laser source is a short pulse Q-switched Nd:YAG laser operated in third harmonic with 196.8-μs time delay. The laser pulse emitted at 355 nm with a repetition rate of 50 Hz. The full width at half-maximum of the pulse is about 5 ns. The maximum energy provided by the laser was 160 mJ per pulse, and a laser energy of 50 mJ per pulse was selected for the experiment. The duration of the Q-switch trigger pulse was 20 μs, which was long enough for the ns-laser pulse. The total data acquisition duration was 25 μs with 10 μs ahead of the Q-switch trigger pulse, which ensured that all information about the spectrum could be captured. Figure 2 shows the temporal parameters for the experiment.

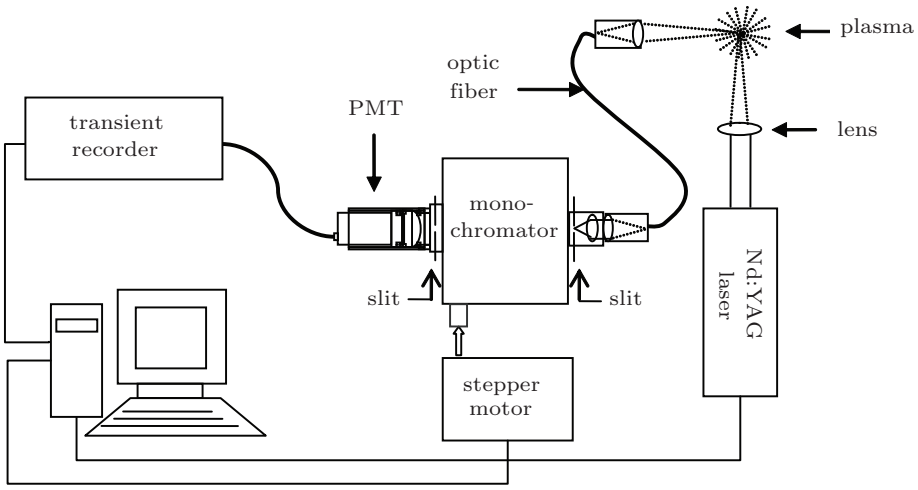


Fig. 1. Schematic plot of the LIBS system consisting of a short-pulse laser, a quartz lens for laser focusing, an optical fiber for light signal collection, a monochromator for selecting the wavelength of light, a stepper motor for changing the measured wavelength, a PMT for photon signal detection and amplification, a transient recorder for data acquisition and processing, and a computer for system automation.

The frequency of the stepper motor and the transient recorder were both set at 50 Hz. In order to synchronize the laser trigger and the transient recorder a reference signal is generated by an external pulse generator via the computer. The PMT high voltage was set at 750 V. The spectral resolution of the monochromator was 0.2 nm. The wavelength interval was 0.0625 nm, which means that the motor ran only one step between two adjacent data acquisition. The data at different wavelengths were collected with two-second integration time which is equivalent to 100 laser-shot exposures. Only analog detection was used, owing to the high intensity of the signals in this particular experiment. The obtained laser excited Raman spectrum of water is shown in Fig. 3.

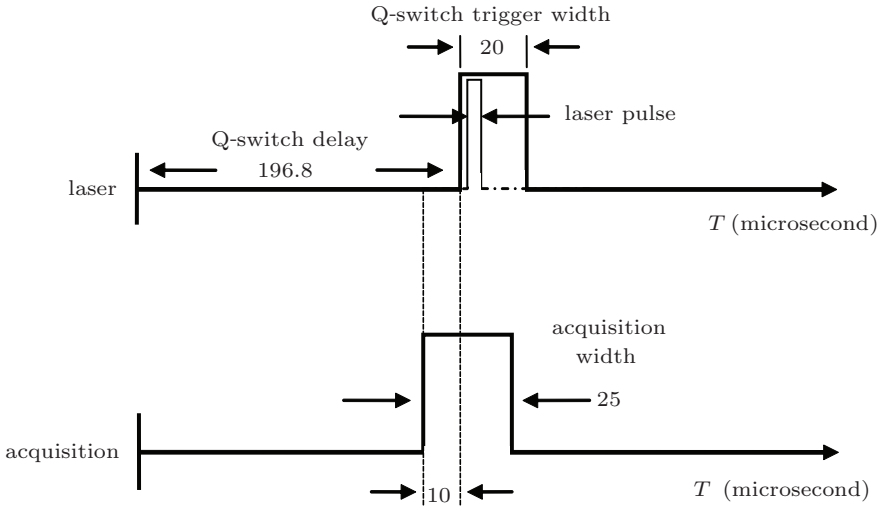


Fig. 2. Temporal parameters for the experiment where the upper panel shows the setting of the laser pulse and the Q-switch trigger, and the laser pulse is delayed after the Q-switch has been triggered by about 180 ns. The lower panel shows the transient recorder parameter with a selected acquisition width long enough for the measurement.

From previous research,[24−30] the signals given in Fig. 3 represent the Raman scattering spectra of both liquid water and water vapour. The focused high energy laser beam was responsible for both evaporating the liquid water and generating the water vapour Raman signal. In order to confirm the phenomena, the optical fiber sub-assembly was moved away from the focal point by a few centimeters along the laser direction and repeated measurements confirmed that the measured spectrum exhibits the liquid water Raman features only, and the strong water vapour Raman spectral features as depicted in Fig. 3 disappeared. Because the laser energy away from the focal spot did not have enough energy density to evaporate the liquid water, only the liquid water Raman spectrum was observed in this area.

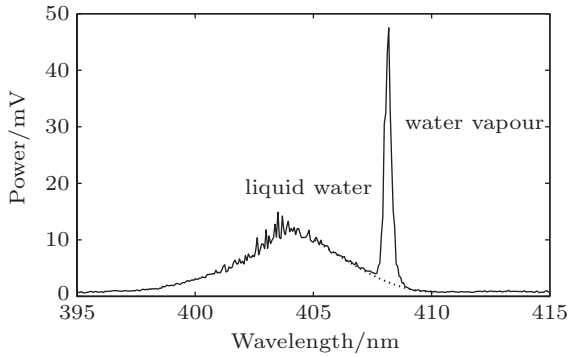


Fig. 3. The Raman scattering spectra of liquid water and water vapour obtained with 355-nm excitation laser. The dotted line represents the liquid water spectrum fitted to a polynomial function of the 3rd order.

In order to check our system further, we compared the water-vapour Raman scattering signal plotted in Fig. 3 with a theoretical calculated result. Because the spectrum in Fig. 3 includes the Raman scattering spectrum of liquid water and water vapour, there are overlap regions between them. In order to get rid of the influence of liquid water, we fitted the liquid water Raman scattering signal to a polynomial function of the 3rd order in the overlap region which is denoted with the dotted line, and subtracted it from the overall spectrum. The result is shown as curve *a* in Fig. 4. It represents a measured water vapour Raman scattering spectrum in the experiment. In Fig. 4, the vibration–rotation simulated Raman scattering spectrum of water vapour is illustrated as curve *b*. The spectra in Fig. 4 have been normalized for comparison.

According to the Lambert law and under the condition of a small signal, the Raman scattering spectral intensity increases linearly with the relating cross sections. Therefore, if we obtain the Raman scattering cross sections, the normalized Raman scattering spectrum is also obtained. Using a rigorous treatment of the relevant perturbations, the ro-vibrational Raman cross sections of an asymmetric top molecule can be obtained from Ref. [24]. The absolute differential scattering cross section $(\partial\sigma/\partial\Omega)$ of the ro-vibrational Raman transition $(0K_{\rm a}K_{\rm c} \rightarrow V'J'K'_{\rm a}K'_{\rm c})$ of H_2O is written as

$$\left(\frac{\partial\sigma}{\partial\Omega}\right)^{[MN]}_{(0K_{\rm a}K_{\rm c}\rightarrow V'J'K'_{\rm a}K'_{\rm c})} = (\upsilon_0-\upsilon)^4\frac{{\rm e}^{-E_i/k_{\rm B}T}}{Z(T)}A^{[MN]}_{(0K_{\rm a}K_{\rm c}\rightarrow V'J'K'_{\rm a}K'_{\rm c})}, \quad (1)$$

where M and N are the polarizations of the incident and scattered photons respectively; υ_0 is the wavenumber of the excited photons; υ is the wavenumber of the Raman shift; E_i is the energy of the starting level; $k_{\rm B}$ is Boltzmann's constant; $Z(T)$ is the total partition function at the absolute temperature T; $A^{[MN]}$ are the coefficients for common experimental scattering geometries.

In the simulation the temperature was 375 K and the incident wavelength was 355 nm, and the other parameters needed were obtained from Tables 6 and 7 in Ref. [24]. The simulated Raman scattering spectrum of water vapour was convoluted to the monochromator transmission factor which is a Gaussian function, then normalized. The result is shown as curve b in Fig. 4.

It can be concluded that the experimental result (curve a) is in agreement with the simulated result (curve b) of water vapour Raman scattering spectrum to a good accuracy, thereby further verifying from such experimental results that the present LIBS system is reliable.

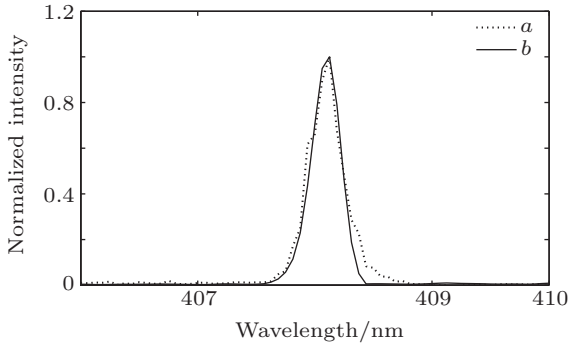


Fig. 4. The comparison between experimental (curve a) and theoretical (curve b) water–vapour Raman scattering spectral lines. Curve a represents the water–vapour Raman line obtained by eliminating the influence of liquid water in the experiment. Curve b refers to the theoretical liquid–water Raman scattering.

3. Experiment and discussion

Using this new LIBS system, a laser induced air breakdown experiment was performed and the air LIBS spectrum was obtained. The wavelength interval was set at 0.25 nm, which means that the motor moved four steps between two adjacent data acquisitions. In the experiment only analog detection was used, owing to the intense air LIBS signals. For each spectral measurement the experimental data were obtained by an accumulation of 150 shots to reduce noise resulting from random shot to shot fluctuation of the laser and other experimental noises. Other experimental parameters were the same as those for the laser induced water–vapour Raman experiment described previously.

Figure 5 illustrates the evolution of the LIBS emission at different wavelengths as a function of time after the Q-switch triggering of the laser. The reference starting time is at the moment when the Q-switch trigger is started. In this figure, the specific lines can be clearly distinguished from the continuum and the spectral line radiation decays can be seen as they disappeared towards the top of the time-resolved spectrograph. Starting at around 0.3 μs after the Q-switch has been started, the individual spectral lines shown as straight lines are clearly visible in the time-resolved spectrograph.

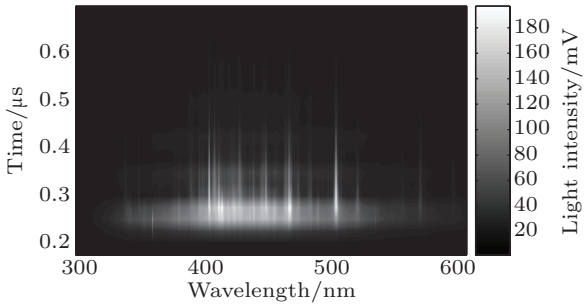


Fig. 5. A computer generated picture of the time-resolved laser induced air breakdown spectrum. After the continuum radiation decayed, the specific emission lines are evident. The maximum intensity of the emission line occurs at about 0.275 μs after the Q-switch trigger has been started. The bright laser pulse intensity line at 355 nm is only visible in this picture for a short duration of a few ns.

In general, the preferred approach in LIBS is to maximize the intensity of the light signal generated for the spectral lines of interest. This can be achieved by adjusting the laser energy used in the LIBS measurement against the time delay after laser emission to obtain an optimized emission signal transient record. In Fig. 5, the signal intensity changes with time at various wavelengths are evident. For a particular application, the appropriate data at different times can be chosen for analysis.

The spectra emitted from plasma at different times are shown in Fig. 6. It is obvious that all the intensities at different wavelengths decay with time. The strong continuum component which appears at earlier times tends to disappear mostly after 0.3 μs. From then, the specific lines which give the information about atomic and molecular de-excitation become more evident. Taking the spectral line at 500.5 nm for example, the signal intensity at this wavelength

changes very slowly with time while the signal intensities at other nearby wavelengths decay quickly.

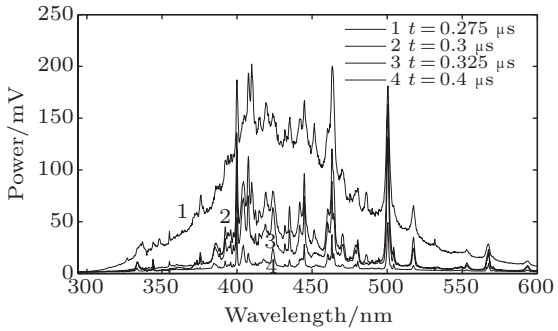


Fig. 6. Emission spectra from the air breakdown plasma at four specific times (0.275, 0.3, 0.325, and 0.4 μs). The four spectra at all wavelengths decay with time and the emission spectral lines decay more evidently at a later time.

The variations of the signal intensity as a function of time for certain lines are shown in Fig. 7, where one can note that these specific lines strongly decrease in intensity. All these lines have a similar decay rate because they are all emitted by nitrogen molecules. Figure 8 gives a single spectrum at 0.45 μs. The discrimination and the analysis of the spectrum are given by the identification software Plasus SpecLine with a spectral resolution of 0.2 nm.

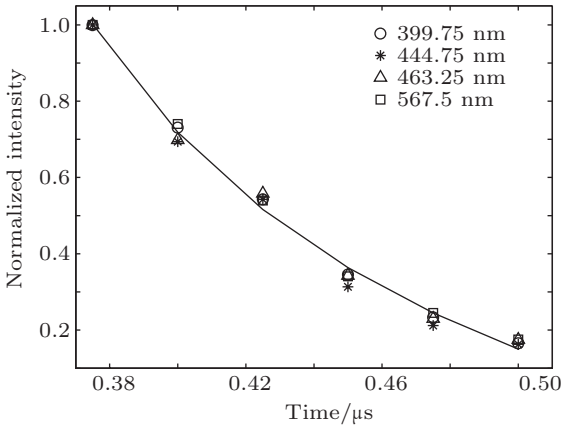


Fig. 7. Variations of the normalized signal intensity with time for lines at different wavelengths (399.75 nm, 444.75 nm, 463.75 nm, and 567.5 nm). The black line is the fitted curve for all the measured data.

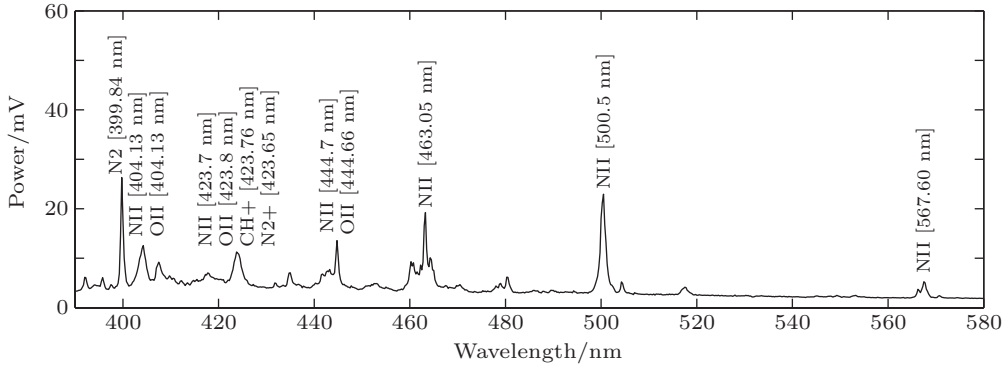


Fig. 8. Single spectrum of laser induced air breakdown at 0.45 μs. The spectral resolution is 0.2 nm.

4. Conclusion

The LIBS technique is a powerful analytical tool, it is sensitive to sample elemental composition, and many trace elements can be detected from their individual spectral line features. The plasma spectrum generated shows unique character and quantity of each substance. In our work, a novel highly-sensitive automatic transient LIBS system is based on the combination of a high power pulse laser, a highly sensitive PMT, a motor driven monochromator, and a computerized transient recorder. This system successfully solves the delay-time selecting problem. It can be used for both LIBS and Raman analysis of different materials. Water Raman scattering measurement is executed to verify the reliability of our system. The obtained experimental data accord well with theoretical water–vapour Raman scattering data. A laser induced air breakdown spectrum is obtained, and experimental results and relevant analyses are given. This system shows a good performance and will be used in other subsequent remote sensing experiments. The use of the current transient recording method together with flash Xenon lamp technology to the DOAS sensing of urban NO_2,[31,32] can allow the monitoring of spatial variation in a range resolution of 30 m–50 m for a width of 0.1 ms–0.17 ms.

Other problems that may be taken into further consideration in LIBS design are interference, self-

absorption, matrix effect, and spectral overlap. Further work will extend to solving these problems, and the applications of LIBS and Raman scattering in atmospheric remote sensing will also be explored.

Acknowledgment

We are indebted to Prof. Ulla Wandinger for the kind help of theoretical Raman scattering calculation.

References

[1] Radziemski L J and Cremers D A 1989 *Laser-Induced Plasmas and Applications* (New York: Marcel Dekker. INC.) pp. 302–317
[2] Colao F, Fantoni R, Lazic V, Paolini A, Fabbri F, Ori G G, Marinangeli L and Baliva A 2004 *Planet. Space Sci.* **52** 117
[3] Senesi G S, Dell'Aglio M, Gaudiuso R, DeGiacomo A, Zaccone C, DePascale O, Miano T M and Capitelli M 2009 *Environ. Res.* **109** 413
[4] Carranza J E, Fisher B T, Yoder G D and Hahn D W 2001 *Spectrochim. Acta* B **56** 851
[5] Zhao P T, Zhang Y C, Wang L, Zhao Y F, Su J, Fang X, Cao K F, Xie J and Du X Y 2007 *Chin. Phys.* **16** 2486
[6] Zhao P T, Zhang Y C, Wang L, Hu S X, Su J, Cao K F, Zhao Y F and Hu H L 2008 *Chin. Phys.* B **17** 335
[7] Sharma S K, Misra A K, Lucey P G and Lentz R C F 2009 *Spectrochim. Acta* A **73** 468
[8] Abraham E, Minoshima K and Matsumoto H 2000 *Opt. Commun.* **176** 441
[9] Giacomo A D, Dell'Aglio M, Colao F, Fantoni R and Lazic V 2005 *Appl. Surf. Sci.* **247** 157
[10] Anijaa M and Philip R 2009 *Opt. Commun.* **282** 3770
[11] Tornari V, Zafiropulos V, Bonarou A, Vainos N A and Fotakis C 2000 *Opt. Lasers Eng.* **34** 309
[12] Stavropoulos P, Michalakou A, Skevis G and Couris S 2005 *Spectrochim. Acta* B **60** 1092
[13] Cui Z F, Zhang X Y, Yao G X, Wang X L, Xu X S, Zheng X F, Feng E Y and Ji X H 2006 *Acta Phys. Sin.* **55** 4506 (in Chinese)
[14] Mansoori A, Roshanzadeh B, Khalaji M and Tavassoli S H 2011 *Opt. Lasers Eng.* **49** 318
[15] Yan L X, Zhang Y S, Zheng G X, Liu J R, Cheng J P and Lü M 2006 *Chin. Phys.* **15** 2271
[16] Shoursheini S Z, Sajad B and Parvin P 2010 *Opt. Lasers Eng.* **48** 89
[17] Travaillé G, Peyrusse O, Bousquet B, Canioni L, Pierres K M L and Roy S 2009 *Spectrochim. Acta* B **64** 931
[18] Wu Y H, Hu H L, Hu S X and Zhou J 2003 *Chin. Opt. Lett.* **1** 373
[19] Goldsmith J E M, Blair F H, Bisson S E and Turner D D 1998 *Appl. Opt.* **37** 4979
[20] Sakai T, Nagai T, Nakazato M, Matsumura T, Orikasa N and Shoji Y 2007 *J. Atmos. Ocean Tech.* **24** 1047
[21] Veselovskii I A, Cha H K, Kim D H, Choi S C and Lee J M 2000 *Appl. Phys.* B **71** 113
[22] Fiorani L, Colao F, Palucci A, Poreh D, Aiuppa A and Giudice G 2010 *Opt. Commun.* **284** 1295
[23] Turner D D and Goldsmith J E M 1999 *J. Atmos. Ocean Tech.* **16** 1062
[24] Avila G, Fernández J M, Maté B, Tejeda G and Montero S 1999 *J. Mol. Spectrosc.* **196** 77
[25] Scherer J R, Go M K and Kint S 1974 *J. Phys. Chem.* **78** 1304
[26] Torii H 2007 *J. Mol. Liq.* **136** 274
[27] Schmidt J R, Roberts S T, Loparo J J, Tokmakoff A, Fayer M D and Skinner J L 2007 *Chem. Phys.* **341** 143
[28] Rull F 2002 *Pure Appl. Chem.* **74** 1859
[29] Murphy W F 1977 *Mol. Phys.* **33** 1701
[30] David D, Strugano A, Bar I and Rosenwaks S 1992 *Appl. Spectrosc.* **46** 1149
[31] Cheng A Y S, Zhu J H and Pau M C Y 2001 *Appl. Spectrosc.* **55** 350
[32] Cheng A Y S and Chan M H 2004 *Appl. Spectrosc.* **58** 1462